Applied Chemical Engineering (2025) Volume 8 Issue 2 ISSN: 2578-2010 (O)
doi: 10.59429/ace.v8i3.5670

ORIGINAL RESEARCH ARTICLE

Exploring the potential of new ligand (-3-((4-(4-((-1,2-diphenyl-2-(thiazol-2-ylimino) ethylidene) amino) benzyl) phenyl) imino) butan-2-mono (PTIEABPBO) type imine-oxime complex with palladium (II) as an anticancer drug

Maysson Hussin Ali[1], Mahmood Oudah mutashar[2], Hussein Abed Al-Hasan[3], Hayder O. Jamel[4*]

[1] *Ministry of Education General Directorate of Al-Qadisiyah Education, Diwaniyah, 58001, Iraq*

[2] *Ministry of Education General Directorate of Maysan Education, Misan, 62010, Iraq*

[3] *Department of Chemistry, College of Science, University of Al-Qadisiyah, Al Diwaniyah, Diwaniyah,,58001,Iraq*

[4*] *Department of Chemistry, College of Education, University of Al-Qadisiyah, Diwaniyah, 58001, Iraq*

***Corresponding author:** Hayder O. Jamel; haider.hassani@qu.edu.iq

ABSTRACT

Herein, a new imine-oxime ligand was synthesized in a two-step reaction. In the first step, 2-aminothiazole and benzil were reacted with glacial acetic acid as a catalyst resulting in the formation of 1,2-diphenyl-2-(thiazol-2-ylimino)ethan-1-one. In the second step, this intermediate was then reacted with diacetyl monoxime and 4,4'-methylenedianiline for synthesis of target ligand, PTIEABPBO. Afterwards, a palladium (II) complex of this ligand was also synthesized. Analyses of ligand and its complex were carried out via FT-IR, UV-Vis, and ^{1}H, ^{13}C-NMR, analysis of melting point, elemental analysis, FESEM, and XRD. Findings of morphological study confirmed the purity of the synthesized compounds by demonstrating close agreement between calculated and experimental values. FT-IR highlights presence of azomethine and oxime bands in ligand, with shifts observed upon complexation with palladium. Crystallographic study indicated a crystalline, nanoscale structure for both compounds. Finally, biological evaluation demonstrated significant inhibitory activity of synthesized compounds against MCF-7 breast cancer cell line, when compared against HEK-293 normal cell line.

Keywords: Anticancer, ligand (LH), Pd (II) complex, cancer cells.

ARTICLE INFO

Received: 13 May 2025
Accepted: 14 June 2025
Available online: 14 July 2025

Highlights

- Synthesis and analysis of nano Schiff base ligand (LH) and its Pd (II) complex
- Square-planar geometry of Pd (II) complex upon coordination with ligand
- Potential against MCF-7 breast cancer cells via MTT assays

Graphical abstract

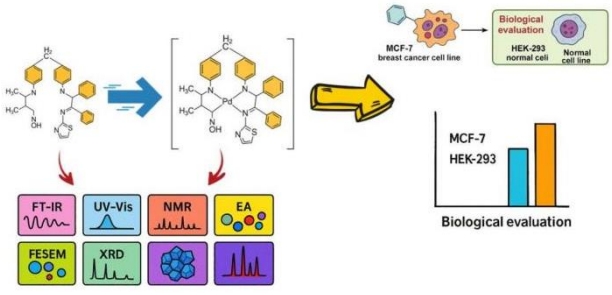

1. Introduction

Oximes and their metal complexes widely studied in coordination chemistry mainly due to the versatile chelating properties of oxime ligand[1,2]. The oxime and oximate forms can coordinate metals in different ways that may include monodentate coordination via nitrogen or oxygen, bidentate chelation via both nitrogen and oxygen as well as bridging coordination by nitrogen and oxygen[3,4]. Schiff base ligands find widespread uses in food, dye, and analytical chemical industries when their complexes were synthesized with transition metal ions[5]. This complexation also improve their biological activities including antifungal and anticancer properties[6]. Studies shown that oximes and their complexes have demonstrated notable biochemical activity[7-12]. Theoretical investigations of oximes and their complexes have become increasingly prevalent in recent years. The synthesis of imine-oximes and their corresponding metal complexes presents a significant challenge within oxime coordination chemistry. These compounds, containing both Schiff base and oxime moieties, attracted considerable attention due to their biological activity and structural characteristics, especially their selective reactivity towards metal ions. However, theoretical studies on imine-oximes and their metal complexes remain relatively rare[13-18]. Oxime-imines denotes class of ligands known for their ability to stabilize metal ions in higher oxidation states. This stabilization is achieved through strong sigma donation from ligand to metal (L→M)[6].

Herein, authors worked on the synthesis of a novel imine-oxime ligand (that was derived from 2-aminothiazole and diacetyl monoxime) in two-step process. In the first step, the compound 1,2-diphenyl-2-(thiazol-2-ylimino) ethan-1-one (A) was synthesized while the second step involved the synthesis of ligand, PTIEABPBO. This synthesized complex was then reacted with palladium (II) ion salt to yield a metal complex. The synthesis of metal-complex was analyzed by Fourier-transform infrared spectroscopy (FT-IR), ultraviolet-visible (UV-Vis) spectroscopy, nuclear magnetic resonance (NMR) spectroscopy (^{1}H and ^{13}C-NMR), analysis of melting point, elemental study (C, H, N), field emission scanning electron microscopy (FESEM), and X-ray diffraction (XRD). The effectiveness of the synthesized metal-ligand complex for biological activity was analysed for breast cancer cell line MCF-7 and a comparative analysis was also conducted against the normal cell line HEK-293.

2. Materials and methods

2.1. Chemicals and materials

All chemicals were supplied by Sigma-Aldrich, Merck, HIMEDIA, and BDH. Ultraviolet-visible (UV-Vis) spectra were recorded in the range of 200–1000 nm (in ethanol solvent) using a Shimadzu U.V-165PCS spectrophotometer. Nuclear magnetic resonance (NMR) spectra were obtained using a Varian Ultra Shield 500 MHz spectrometer (Switzerland), operating at 500 MHz, with tetramethylsilane (TMS) as the internal standard and DMSO-d6 as the solvent. Fourier-transform infrared analysis was carried out via Shimadzu FTIR 8400S spectrophotometer (400–4000 cm^{-1}). Melting points analyzed using a Stuart melting point apparatus. Magnetic susceptibility measurements carried out at room temperature via the Faraday method through Magnetic Susceptibility Balance Model M.S.B Auto. The metal content in the complexes was determined through flame atomic absorption spectroscopy. The molar conductivities of the prepared metal complex solutions dissolved in absolute ethanol were measured with a Cond.720 conductivity meter (WTW) equipped with a platinum electrode. X-ray diffraction (XRD) patterns for the synthesized ligand and its complex were obtained using a Bestic aluminium anode XRD system. Additionally, magnified images of the synthesized ligand and its complex were captured using a TESCAN MIRA3 scanning electron microscope (Czech Republic).

2.2. Synthesis Procedure

The ligand (PTIEABPBO) was synthesized in two steps:

Step 1: Synthesis of Compound (A): 1,2-diphenyl-2-(thiazol-2-ylimino) ethan-1-one

A solution was prepared by dissolving 2-aminothiazole (1.00 g, 0.01 mol) in 25 mL absolute ethanol. Separately, benzil (2.1 g, 0.01 mol) was dissolved in 25 mL of absolute ethanol, and 5–6 drops glacial acetic acid were mixed with benzil solution. After combining the two solutions, mixture was heated under reflux for eight hours, followed by cooling, filtration and drying. This crude product was further purified by recrystallization from hot ethanol afterwards, it was filtered, dried, and weighed. The final yield was 76%, with melting point in between 94 and 97 ℃.

Step 2: Synthesis of the Ligand (PTIEABPBO)

Diacetyl monoxime (1.01 g, 0.01 mol) and 4,4'-methylenedianiline (1.98 g, 0.01 mol) were each dissolved separately in 25 mL of anhydrous ethanol. A third solution was prepared by dissolving Compound A (2.92 g, 0.01 mol) in 25 mL of ethanol. Five to six drops of glacial acetic acid were added to diacetyl monoxime and Compound A solution. These three solutions were then combined, and the resulting mixture was heated under reflux for eight hours followed by cooling. The resulting precipitate was collected by filtration, dried, and recrystallized from ethanol. The purified product was obtained with an 80% yield with melting point between 103 and 105 ℃ (**Figure 1**).

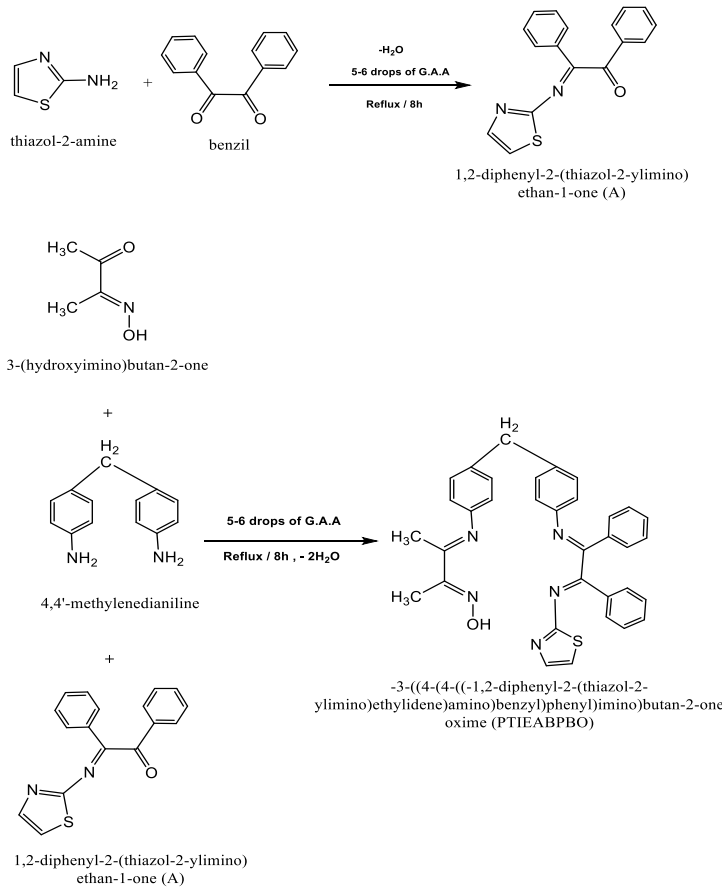

Figure 2. Synthesis of novel imine - oxime ligand (PTIEABPBO).

2.3. Synthesis of Complex

For complex synthesis, ligand (0.694 g, 1 mmol) added to 10 mL ethanol followed by addition to palladium(II) chloride (0.17 g, 1 mmol) dissolved in 5 mL of distilled water. Mixture was refluxed with continuous stirring for 2 hours, during which precipitate formation take place. The reaction mixture was undergoing cooling, filtration and drying. Recrystallization from absolute ethanol yielded colored precipitate. The product had a melting point of 173–176 ℃ and a yield of 85%.

2.4. Biological Activity Analysis

2.4.1. Biological activity

a) Cytotoxicity assays: Cell lines

Herein, breast cancerous cell line MCF-7 and normal cell line HEK-293 were utilized. All cell lines were maintained and cultured under appropriate conditions, and the necessary assays were performed on them.

b) Cultivation of MCF-7 breast cancer cell line

The method described by Freshney (1) was employed to culture MCF-7. The frozen cells were thawed in a water bath maintained at 37 ℃. The cancer cells were cultured using a 25 cm^2 animal cell culture flask containing Dulbecco's Modified Eagle Medium (DMEM) supplemented with 10% fetal bovine serum (FBS). The flasks were incubated in a 5% CO_2 incubator at 37°C for one day. After incubation period, to ensure proper cell growth and absence of contamination, secondary cultures were prepared.

Microscopic examination of all cell cultures was performed using an inverted microscope to verify cell viability, confirm the absence of contamination, and assess cell growth. Acceptable cultures exhibited cell densities between 500,000 and 800,000 cells/mL. Afterwards, cell cultures were transferred to a biosafety cabinet, and spent culture medium was carefully aspirated. The cells were then washed twice with physiological saline solution (PBS) for ten min. An appropriate volume of trypsin enzyme was then added to the cells, followed by incubation at 37 ℃ for 30–60 seconds. The cells were observed until they detached from the surface and transitioned from a monolayer to single cells. The enzymatic action of trypsin was halted by adding fresh growth medium supplemented with FBS. The cells were collected in centrifuge and supernatant was then discarded while the cells were resuspended in fresh growth medium that contains 10% FBS. A portion of the resuspended cells was analyzed to determine the total cell count and viability. Equal volumes of the cell suspension and Trypan Blue stain were mixed and examined using a hemocytometer, with the following formula used to calculate cell viability:

$$C = N \times 10^4 \times F\ /ml \tag{1}$$

$$Viability\ \% = (live\ cells\ /\ dead\ cells) \times 100 \tag{2}$$

Here, C represent cell count per mL, F = dilution factor, and N = number of cells counted on slide. The constant 10^4 accounts for slide's dimensions. Following preparation, cell suspension was aliquoted into new vessels and undergo incubation overnight (37 ℃).

2.4.2. MTT dye test for cell viability

a) Experimental procedure

Cancer cell lines were seeded into a 96-well flat-bottom plate. The plate was incubated for 24 hours at 37 °C in a 5% CO_2 atmosphere. Following incubation, 100 µL of cell suspension added to each well. Subsequently, concentrations of compounds studied (15.625, 31.25, 62.5, 125, 250, 500 µg/mL) were added to the wells, with each concentration applied to three wells. The plate was then incubated for another 24 hours at 37 ℃. Following the incubation, 10 µL of 3-(4,5-dimethylthiazol-2-yl)-2,5-diphenyltetrazolium bromide (MTT) solution, at a concentration of 0.5 mg/mL, was added to each well. Following the initial incubation, plate was incubated for a further four hours (37 ℃) to allow formazan crystal formation. Subsequently, 100 µL of solubilization solution was added to each well to dissolve formed crystals. Absorbance was measured at 570 nm by microplate reader. These readings are proportional to number of viable cells present.

3. Results and Discussion

3.1. Physico-chemical characteristics

The synthesized ligand, a yellow crystalline substance, exhibited a color change upon reaction with palladium ions. The resulting palladium (II) complex was brown and stable at room temperature. Further characteristics of ligand and its complex are presented in **Table 1**.

Table 1. Properties of LH and its complex.

Compound	M. Wt g/mol	Color	MP (C)	Yield %	Calc. (Found)%				
					C	H	N	S	M
PTIEABPBO $C_{34}H_{29}N_5OS$	555.70	orange	103-105	80.20	73.49 (74.14)	5.26 (5.31)	12.60 (12.92)	5.77 (5.84)	—
[Pd(PTIEABPBO)]Cl_2 $C_{34}H_{29}Cl_2N_5OPdS$	733.02	brown	173-176	85.5	55.71 (56.15)	3.99 (4.03)	9.55 (9.74)	4.37 (4.43)	14.52 (14.73)

3.2. NMR results

(a) Proton Nuclear Magnetic Resonance Spectrum of Ligand (PTIEABPBO)

The ^{1}H-NMR spectrum of the newly synthesized ligand (PTIEABPBO) was recorded using DMSO-d_6 as the solvent and TMS (**Figure 2**). The spectrum possess a singlet at δ:2.182 ppm (S,3H), corresponding to methyl group protons attached to azomethine group (-N=C−CH_3). Additionally, a singlet observed at δ:2.005 ppm (S,3H) was attributed to the protons of the methyl group linked to oxime azomethine group (HO−N=C−CH_3)[3]. A singlet at δ:3.979 ppm (S,2H) was assigned to the methylene protons (−CH_2−). The doublets at δ:7.268 ppm (D,2H) and δ:7.180 ppm (D,2H) was attributed to the protons of the phenyl ring attached to the methine group[4]. Multiplets in the range of δ:7.564–7.968 ppm (M,10H) were assigned to the protons of the two phenyl rings of benzil, while Multiplets at δ:7.524–7.830 ppm (M,2H) were associated with the protons of the thiazole ring[5]. A singlet at δ:12.028 ppm (S,1H) corresponded to the hydroxyl group of the oxime (OH)[6]. Additionally, the signal at δ: 2.520 ppm was identified as originating from the protons of the solvent (DMSO-d_6)[7].

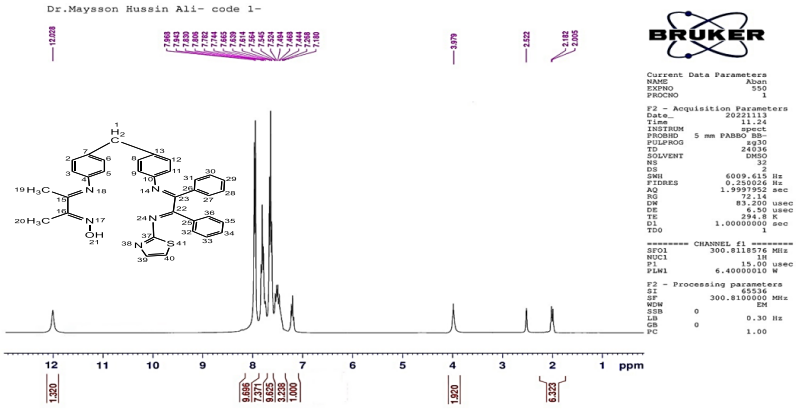

Figure 2. The ^{1}H-NMR of PTIEABPBO

(b) 13C Nuclear Magnetic Resonance Spectrum of Ligand (PTIEABPBO)

This Section describes the ^{13}C-NMR spectrum of the ligand (PTIEABPBO), as illustrated in **Figure 3**. The spectrum revealed several distinct signals, detailed as follows: The ligand (PTIEABPBO) exhibited two signals at δ:10.298 ppm and δ:14.245 ppm, corresponding to C20 and C19 of methyl (−N=C−CH_3) and (O−N=C−CH_3), respectively[8]. A signal observed at δ: 45.298 ppm was attributed to C1[9], the carbon atom of the methylene group (−CH_2−). additionally, signals at δ: 136.005 ppm, δ: 130.085 ppm, δ: 120.623 ppm, δ: 139.182 ppm, and δ: 146.852 ppm were associated with the carbon atoms C7,C13, C12,C8,C6,C2,

C11,C9,C5,C3, C4, and C10, respectively, belonging to the phenyl rings linked to the methylene group[10]. Signals at δ:134.327 ppm, δ:129.341 ppm, δ:128.870 ppm, and δ:132.403 ppm corresponded to the carbon atoms C26,C25, C36,C32,C31,C27, C35,C33,C30,C28 and C34,C29 attributed to the phenyl rings oof benzil[11]. Furthermore, signals at δ:136.368 ppm, δ:114.439 ppm, and δ:166.086 ppm were linked to the carbon atoms C39,C40 and C37 of the thiazole ring[12]. Finally, signals at δ:165.924 ppm, δ:147.365 ppm, and δ:147.099 ppm were ascribed to the carbon atoms C15,C16 and C23,C22 respectively, corresponding to the azomethine groups[13].

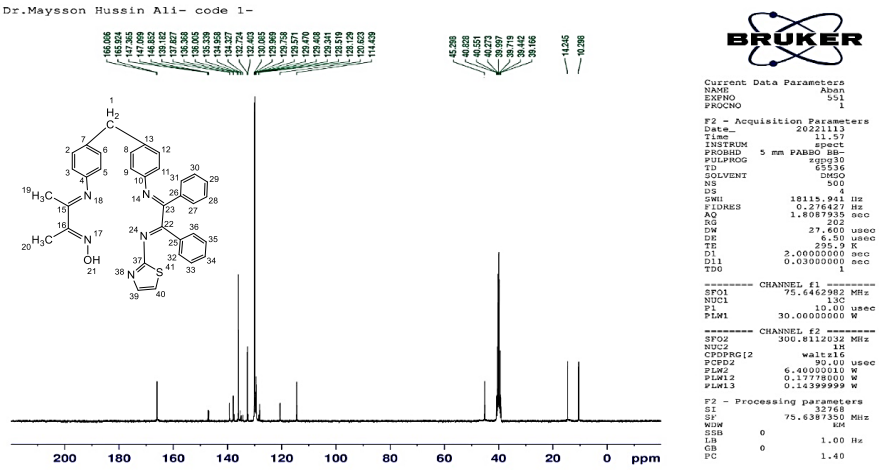

Figure 3. The ^{13}C-NMR of ligand.

3.3. FTIR results

FT-IR helps to identify the functional groups present in studied sample [19-25]. The spectrum displayed a band at 3440 cm^{-1}, attributed to the υ(O–H) group of the oxime. Bands centered at 3062 cm^{-1} and 2970, 2923, 2854 cm^{-1} were assigned to the υ(C–H) stretching vibrations of the aromatic and aliphatic groups, respectively. The bands observed at 1681 cm^{-1} and 1666 cm^{-1} corresponded to the υ(C=N) stretching vibrations of the imine and oxime azomethine groups, respectively. The υ(C=N) stretching vibration of the thiazole ring appeared as a band at 1596 cm^{-1}. Additional bands at 1512 cm^{-1} and 1450 cm^{-1} were assigned to the υ(C=C) stretching vibrations of the aromatic groups. Bands at 1211 cm^{-1} and 1018 cm^{-1} were attributed to the υ(C–N) and υ(C–S) vibrations of thiazole ring, respectively[23,26-29]. When comparing the FT-IR spectrum of the free ligand (PTIEABPBO) with that of its complex, shifts in some bands and the appearance of new bands were observed[27-29], indicating coordination between the metal and the ligand. The azomethine (Schiff base) group frequency, which appeared at 1681 cm^{-1} in the spectrum of the free ligand, shifted to a lower frequency at 1672 cm^{-1} in the spectrum of the synthesized complex. Similarly, the frequency of the oxime azomethine group shifted to a lower frequency, decreasing by 16 cm^{-1}. In contrast, the oxime hydroxyl group showed no significant change, indicating its non-involvement in coordination . New bands were observed at 555 cm^{-1}, corresponding to the M–N bond. **Table 2** and **Figure 4a-b** summarizes the key and significant bands observed in the FT-IR spectra of the ligand (PTIEABPBO) and its palladium complex .[27-30,31]

Table 2. FTIR results of PTIEABPBO and its complex.

Compound	υ(O-H) oxime	υ (C-H) aromatic υ (C-H) aliphatic	υ(C=N) imine υ(C=N) oxime	υ(C=N) Thiazole ring	υ(C=C) aromatic ring	υ(M-N)
Ligand (PTIEABPBO)	3440	3062 2970 , 2923 , 2854	1681 1666	1596	1512 , 1450	—
[Pd(PTIEABPBO)]Cl$_2$	3440	3062 2970 , 2903 , 2832	1672 1650	1596	1512 , 1450	555

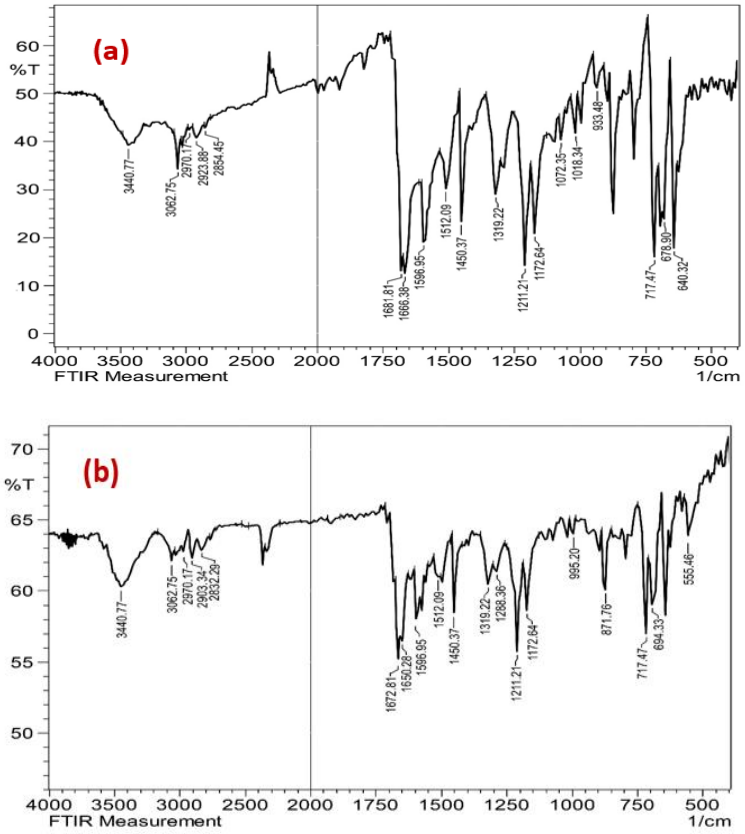

Figure 4. FTIR of PTIEABPBO (a) and its complex (b)

3.4. Electronic spectra and molar conductivity analysis

The electronic spectrum of PTIEABPBO show three peaks at 204 nm (49020 cm^{-1}), 258 nm (38760 cm^{-1}), and 327 nm (30581 cm^{-1}). The first two peaks were attributed to π-π* transitions, while the third peak corresponded to the n-π* transition associated with the azomethine group (C=N).In spectrum of palladium (II) complex, absorption peaks were observed at 221 nm (45249 cm^{-1}) and 294 nm (34014 cm^{-1}). These peaks were assigned to ligand-centered transitions. Additional absorption peaks were observed at 508 nm (19685 cm^{-1}), 582 nm (17182 cm^{-1}), and 654 nm (15291 cm^{-1}), corresponding to transitions $^1A_1g \rightarrow {}^1E_1g$, $^1A_1g \rightarrow {}^1B_1g$, and $^1A_1g \rightarrow {}^1A_2g$, respectively. These transitions confirmed that the complex adopts a square planar geometry. Magnetic susceptibility measurements indicated that all the d-orbital electrons were paired, resulting in a low magnetic moment value close to zero. This finding corresponds to the electronic configuration $t_2g^6e_xg^2$ and suggests dsp ^{2}hybridization (**Table 3** and **Figure 5a-b**).

Table 3. UV-Vis peaks, magnetic momentum µeff (B.M) and supposed geometries for ligand and its complex.

Compounds	λ (nm)	υ^- (cm^{-1})	Transitions	µeff (B.M)	Geometry
Ligand (PTIEABPBO)	204	49020	π-π*	——	——
	258	38760	π-π*		
	327	30581	n-π*		
[Pd(PTIEABPBO)]Cl_2	221	45249	Intra Ligand	(Dia.)	Square planar dsp^2
	294	34014	Intra Ligand		
	508	19685	$^1A_1g \rightarrow {}^1Eg$		
	582	17182	$^1A_1g \rightarrow {}^1B_1g$		
	654	15291	$^1A_1g \rightarrow {}^1A_2g$		

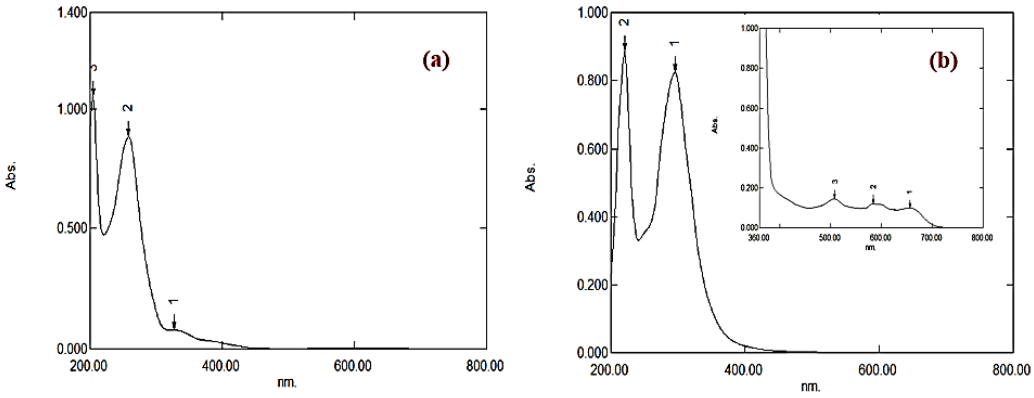

Figure 5. The electronic results of PTIEABPBO (a) and its complex (b).

3.5. Structural analysis

SEM is widely employed method for getting information regarding morphology, particle size, shape[32,33] as well as aggregation in sample. Herein, SEM study was carried out for both ligand and its complex. For conducting analysis, cross-sectional distance of 500 nm and a magnification power of K X Mag = 70.00. SEM images of ligand were used that showed the presence of spherical and heterogeneous granules in studied samples having an average particle size of 45.445 nm (**Figure 6a-b**). Furthermore, SEM of palladium (II) complex revealed spherical particles with size of particles as 63.89 nm that showed the variations between ligand and its complex.

Elemental microanalysis was performed to determine the carbon, hydrogen, nitrogen, and sulfur content of LH and its complex. This analysis is useful in determination of chemical formulas of both compounds. Findings showed that experimentally determined elemental ratios were in close agreement with theoretically calculated values, that revealed the proposed structures and compositions of LH and its complex, as illustrated in **Figure 7a-b**, correspondingly.

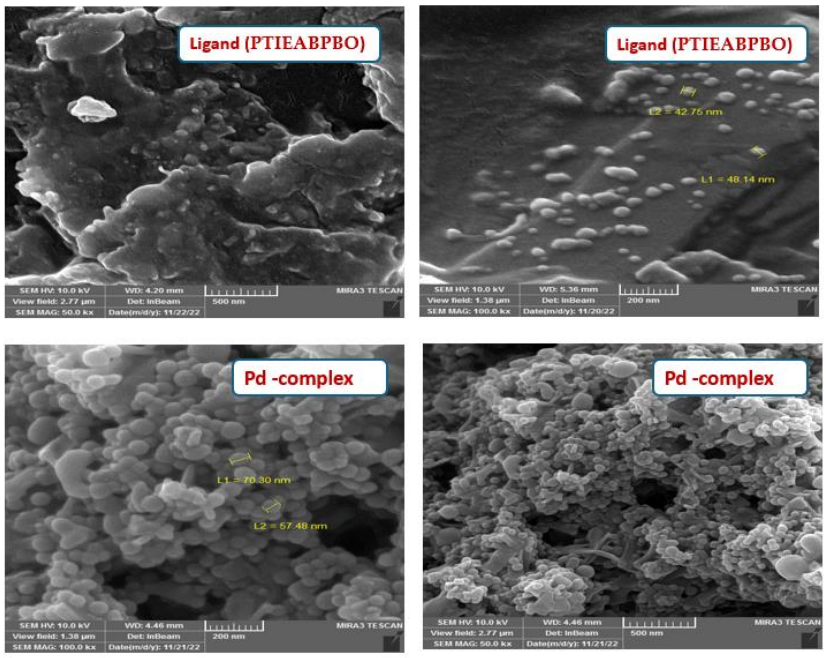

Figure 6. FESEM of PTIEABPBO (a) and its complex (b).

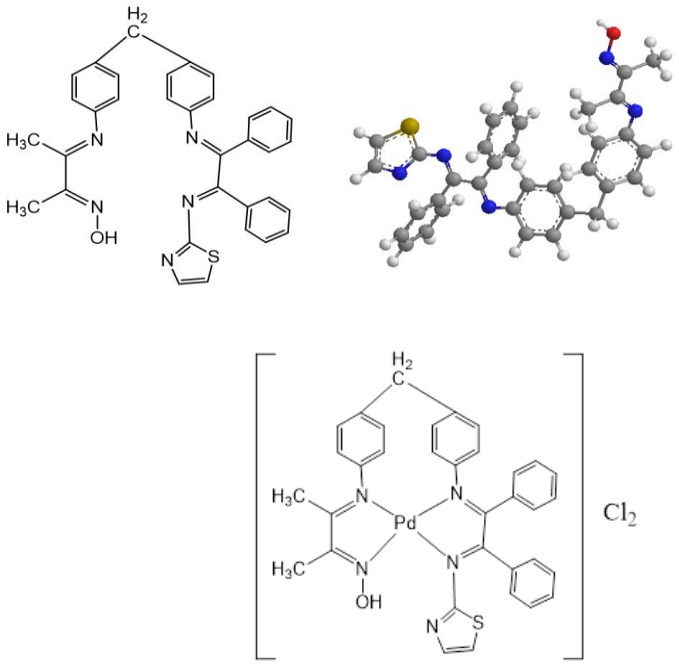

Figure 7. Proposed and 3D structure of PTIEABPBO (a) and its complex (b).

3.6. Crystallographic study

X-ray diffraction (XRD) [34,35] [15,16] was used to investigate the solid-state crystalline structures of PTIEABPBO and its complex (2θ = 10° to 80°). Results showed crystalline nature, crystallite size, and purity of compounds. It was observed that several factors can contribute to broadening of XRD peaks such as micro-strains (like lattice deformation), crystal faults and distribution of these domain sizes. Herein, XRD spectra confirmed the crystalline nature of all compounds. Further, PTIEABPBO revealed sharp, well-defined peaks that clearly showed the presence of highly crystalline structure. Also, palladium (II) complex displayed sharp crystalline peaks, further corroborating its crystalline nature (**Figure 8** and **Table 4-5**).

Table 4. Diffraction angles 2θ, d-spacing as well as relative intensities (rel. Int.%) for both PTIEABPBO and its complex.

COMPOUND	NO.	POS. °2Θ.(RADIAN)	D-SPACE IN A°	INTENSITY IN	[%] REL. INT
LIGAND (PTIEABPBO)	1-	24.488	3.6323	890	100 %
	2-	25.388	3.5055	808	70%
	3-	12.268	7.2089	762	56%
	4-	22.224	3.9969	737	51.0%
	5-	17.805	4.9779	883	34%
[PD(PTIEABPBO)]CL_2	1-	25.344	3.5114	1772	100 .0%
	2-	17.785	4.9832	1083	76%
	3-	24.412	3.6433	1357	50%
	4-	22.065	5.0253	1602	46%
	5-	12.159	7.2735	1648	26%

Table 5. Diffraction angles, width of peaks at mid-intensity, and crystal size for both PTIEABPBO and its complex.

COMPOUND	NO.	PEAK POSITION ²Θ	PEAK WIDTH (FWHM)	D CRYSTALLITE SIZE(NM)	REL. INT . [%]	LATTICE STRAIN
LIGAND (PTIEABPBO)	1-	24.536	0.159	53.42	100%	0.0032
	2-	25.398	0.096	88.64	70%	0.0019
	3-	12.243	0.149	56	56%	0.0061
[PD(PTIEABPBO)] CL_2	1-	25.321	0.010	50.8	100%	0.002
	2-	24.446	0.222	38.26	75%	0.0045
	3-	17.7	0.178	47.2	50%	0.0050

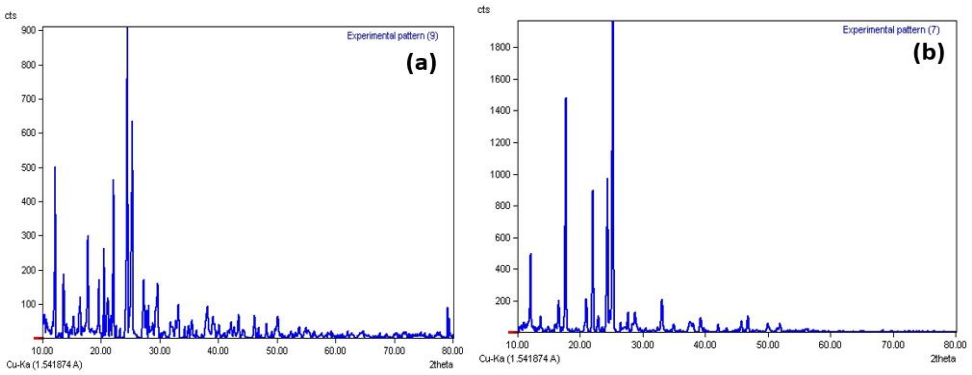

Figure 8. XRD of PTIEABPBO (a) and its complex (b).

3.7. Cytotoxicity test

Chemotherapy is the most common treatment for many types of cancer. The MTT assay was employed to measure cell viability. At 1600 µg/mL, PTIEABPBO repressed growth of breast cancer cells (MCF-7) by 83.20% and normal cells by 89.15%. The lowest inhibition by the ligand was observed at a concentration of 50 µg/mL, with 18.25% inhibition for MCF-7 cells and 13.45% for normal cells. The palladium complex demonstrated the highest inhibitory efficiency against MCF-7 cells at a concentration of 1600 µg/mL, achieving 99.85% inhibition. At the same concentration, it showed 94.60% inhibition of normal cells (HEK-293). The lowest inhibition by the complex was observed at a concentration of 50 µg/mL, with 53.54% inhibition for MCF-7 cells and 7.65% inhibition for normal cells (**Table 6-7** and **Figure 9-10**).

Table 6. PTIEABPBO for MCF-7 and HEK-293 (average±standard deviation (S.D)). IC50 values were estimated graphically using dose-response curves; units in µg/mL.

LIGAND (PTIEABPBO)				
CONCENTRATION µG/ML	Cancer cell MCF-7 Cell Viability mean ±SD	Cell inhibition %	Normal cell HEK-293. Cell Viability mean ±SD	Cell inhibition %
0	100.00 ±0	0.00	100.00 ±0	0.00
50	81.75 ±2.05	18.25	86.55 ±1.20	13.45
100	62.20 ±2.82	37.80	63.75 ±1.34	36.25
200	43.95 ±5.16	56.05	63.83 ±10.57	36.17
400	41.55 ±5.72	58.45	48.68 ±7.24	51.32
800	33.95 ±3.88	66.05	35.18 ±0.31	64.82
1600	16.80 ±0	83.20	10.85 ±6.43	89.15
IC50	5.32		5.84	

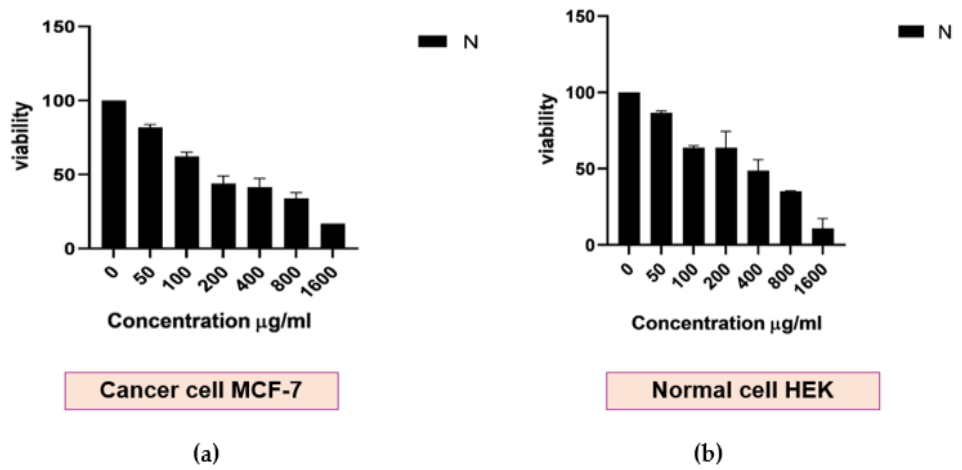

Figure 9. Cytotoxicity of PTIEABPBO for MCF-7 and HEK-293 cell line as cell viability (a) and % cell inhibition (b)

Table 7. Pd (II) complex of ligand for MCF-7 and HEK-293 (average±standard deviation (S.D)). IC50 values were estimated graphically using dose-response curves; units in µg/mL.

PD (II) COMPLEX				
CONCENTRATION µG/ML	**Cancer cell MCF-7**		**Normal cell HEK-293.**	
	Cell Viability mean ±SD	**Cell inhibition %**	**Cell Viability mean ±SD**	**Cell inhibition %**
0	100.00 ±0	0.00	100.00 ±0	0.00
50	46.55 ±1.06	53.45	92.35 ±2.89	7.65
100	19.80 ±0.84	80.20	45.00 ±3.11	55.00
200	12.55 ±5.16	87.45	21.30 ±3.25	78.71
400	13.05 ±5.86	86.95	17.72 ±0.01	82.28
800	6.10 ±0.70	93.90	12.30 ±5.09	87.70
1600	0.15 ±0.07	99.85	5.40 ±1.69	94.60
IC50	0.475		1.30	

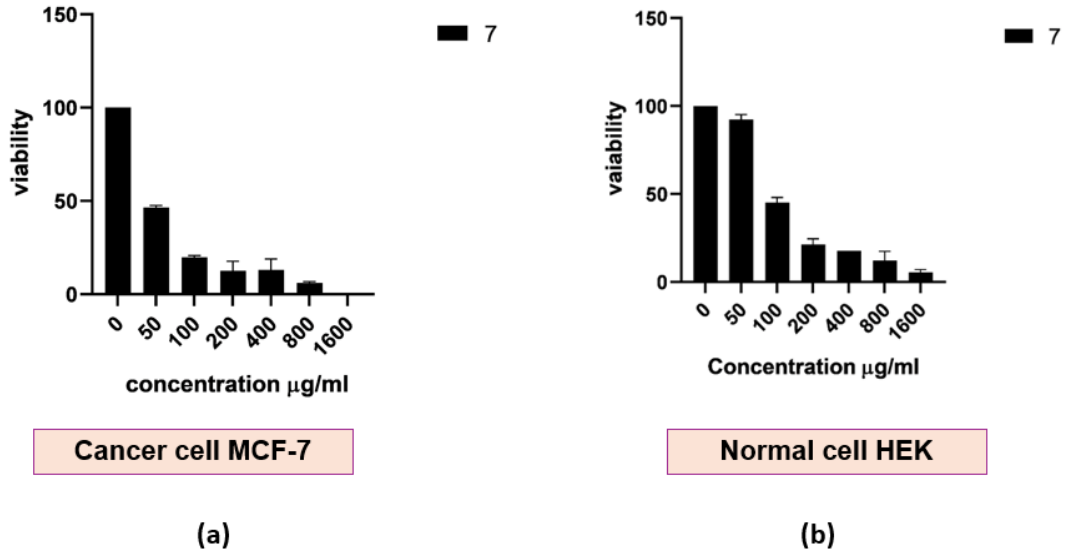

Figure 10. Cytotoxicity of complex of against MCF-7 and HEK-293 as cell viability (a) and % cell inhibition (b).

4. Conclusions

The spectroscopic and analytical measurements conducted on the ligand (PTIEABPBO) and its Pd (II) complex demonstrated that molar ratio for complex with the ligand is 1:1 [M:L]. The molar conductivity value of the palladium (II) complex indicated its ionic nature with a 2:1 ratio. The above findings confirmed that the geometric structure of the palladium (II) complex is square planar. Infrared spectroscopy revealed that LH coordinates with metal ion through nitrogen atoms of the imine and oxime azomethine groups, functioning as a tetradentate ligand. Field emission scanning electron microscopy (FESEM) images showed that both the ligand and its complex possess crystalline and granular structures with particle sizes below 100 nm, indicating they fall within the nanoscale range. These characteristics highlight their potential importance in medical and industrial applications. X-ray diffraction (XRD) analysis further confirmed that the ligand and its complex exhibit a crystalline structure with a defined lattice network and nanoscale features. MTT cytotoxicity assays revealed that the palladium complex derived from the ligand (HL) exhibited high selectivity in killing breast cancer cells (MCF-7) while exerting a less significant effect on normal cells.

Author contributions

Authors contributed equally to the manuscript.

Acknowledgments

Authors would like to acknowledge University of Al-Qadisiyah for administrative and technical support.

Conflict of interest

The authors declare no conflict of interest

References

1. Milios CJ, Stamatatos TC, Perlepes SP. The coordination chemistry of pyridyl oximes. Polyhedron. 2006;25(1):134-94.
2. Keeney M, Osseo-Asare K, Woode K. Transition metal hydroxyoxime complexes. Coord Chem Rev. 1984;59:141-201.
3. Audhya A, Bhattacharya K, Maity M, Chaudhury M. Building Metallacrown Topology around a Discrete [M3 (μ3-O)](M= Ni (II) and Pd (II)) Core Using Oximato Oxygen Linkers: Synthesis, Structures, and Spectroscopic Characterization of a New Family of Compounds with an Inverse-9-MC-3 Motif. Inorg Chem. 2010;49(11):5009-15.
4. Fierro CM, Smith PD, Horton PN, Hursthouse MB, Light ME. Synthesis and structures of mono and binuclear nickel (II) thiolate complexes of a dicompartmental pseudo-macrocycle with N (imine) 2S2 and N (oxime) 2S2 metal-binding sites. Inorg Chim Acta. 2011;368(1):257-62.
5. Chohan ZH, Sumrra SH, Youssoufi MH, Hadda TB. Metal based biologically active compounds: Design, synthesis, and antibacterial/antifungal/cytotoxic properties of triazole-derived Schiff bases and their oxovanadium (IV) complexes. European journal of medicinal chemistry. 2010;45(7):2739-47.
6. Al-Mamaary S, Idrees O, Al-Ta'yy M, Adolrazzaq M, Jirjees HM. Novel Schiff Base Monoxime Complexes: Synthesis, Characterization, Antibacterial Study, and Surface Properties. Iran J Chem Chem Eng(IJCCE) Research Article Vol. 2024;43(10).
7. Quiroga AG, Cubo L, de Blas E, Aller P, Navarro-Ranninger C. Trans platinum complexes design: One novel water soluble oxime derivative that contains aliphatic amines in trans configuration. J Inorg Biochem. 2007;101(1):104-10.
8. Scaffidi-Domianello YY, Meelich K, Jakupec MA, Arion VB, Kukushkin VY, Galanski MS, et al. Novel cis-and trans-configured bis (oxime) platinum (II) complexes: synthesis, characterization, and cytotoxic activity. Inorg Chem. 2010;49(12):5669-78.
9. Abdulsahib WK, Ganduh SH, Radia ND, Jasim LS. New approach for sulfadiazine toxicity management using carboxymethyl cellulose grafted acrylamide hydrogel. International Journal of Drug Delivery Technology. 2020;10(2):259-64.

10. Ganduh SH, Aljeboree AM, Mahdi MA, Jasim LS. Spectrophotometric Determination of Metoclopramide-HCL in the Standard Raw and it Compared with Pharmaceuticals. Journal of Pharmaceutical Negative Results. 2021;12(2):44-8.
11. Al-Suraify SMT, Mekky AH, Husssien LB. Synthesis of new nitrogenous derivatives based on 3-chloro–1-methyl-1H-indazole. International Journal of Pharmaceutical Research. 2020;12:793-802.
12. AlSaadi EK, Darweesh MA, Al Jawadi HF, Othman MAM. Demographic Characteristics, Clinical Features, Laboratory, and Radiological Findings in Children Admitted to COVID19 Center in Amara City, Misan Province, Iraq. Journal of Medicinal and Chemical Sciences. 2023;6(1):34-43.
13. Jayaseelan P, Prasad S, Vedanayaki S, Rajavel R. Synthesis, spectral characterization, electrochemical and anti-microbial activities of new binuclear Schiff base metal complexes derived from 3, 3'diaminobenzedine. European Journal of Chemistry. 2011;2(4):480-4.
14. Maity D, Chattopadhyay S, Ghosh A, Drew MG, Mukhopadhyay G. Syntheses, characterization and X-ray crystal structures of a mono-and a penta-nuclear nickel (II) complex with oximato Schiff base ligands. Inorg Chim Acta. 2011;365(1):25-31.
15. Koumousi ES, Zampakou M, Raptopoulou CP, Psycharis V, Beavers CM, Teat SJ, et al. First palladium (II) and platinum (II) complexes from employment of 2, 6-diacetylpyridine dioxime: synthesis, structural and spectroscopic characterization, and biological evaluation. Inorg Chem. 2012;51(14):7699-710.
16. Kaya Y, Icsel C, Yilmaz VT, Buyukgungor O. A palladium (II) complex containing both carbonyl and imine oxime ligands: Crystal structure, experimental and theoretical UV–vis, IR and NMR studies. Spectrochimica Acta Part A: Molecular and Biomolecular Spectroscopy. 2013;108:133-40.
17. Bdaiwi ZM, Ghanem HT. Synthesis and characterization of some heterocyclic derivatives from 2-amino thiazol and study of biological activity of prepared derivatives. International Journal of Pharmaceutical Research. 2020;12(2):1207-16.
18. Khliwi FS, Alshamsi HA. Design of a Z-Scheme System with g-C3N4/WO3/ZnFe2O4 Nanocomposite for Photocatalytic Degradation of Rhodamine B. Journal of Cluster Science. 2025;36(3).
19. Shah A, Arjunan A, Manning G, Batool M, Zakharova J, Hawkins AJ, et al. Sequential novel use of Moringa oleifera Lam., biochar, and sand to remove turbidity, E. coli, and heavy metals from drinking water. Cleaner Water. 2024;2:100050.
20. Shah A, Arjunan A, Thumma A, Zakharova J, Bolarinwa T, Devi S, et al. Adsorptive removal of arsenic from drinking water using KOH-modified sewage sludge-derived biochar. Cleaner Water. 2024;2:100022.
21. Imran MS, Javed T, Areej I, Haider MN. Sequestration of crystal violet dye from wastewater using low-cost coconut husk as a potential adsorbent. Water Science and Technology. 2022;85(8):2295-317.
22. Jamel HO, Jasim MH, Mahdi MA, Ganduh SH, Batool M, Jasim LS, et al. Adsorption of Rhodamine B dye from solution using 3-((1-(4-((1H-benzo [d] imidazol-2-yl) amino) phenyl) ethylidene) amino) phenol (BIAPEHB)/P (AA-co-AM) composite. Desalination and Water Treatment. 2025:101019.
23. Hosseini M, Ghanbari M, Dawi EA, Mahdi MA, Ganduh SH, Jasim LS, et al. Investigations of nickel silicate for degradation of water-soluble organic pollutants. International Journal of Hydrogen Energy. 2024;61:307-15.
24. Bdaiwi ZM, Abbas GJ, Ghanem HT. Synthesis, Characterization of Heterocyclic Compounds Containing Dapsone. International Journal of Drug Delivery Technology. 2022;12(3):1446-52.
25. Bdaiwi ZM, Ghanem HT. Synthesis and characterization of some oxazepine compounds from 2- amino thiazole. Journal of Global Pharma Technology. 2020;12(6):291-303.
26. Atyaa AI, Radhy ND, Jasim LS, editors. Synthesis and Characterization of Graphene Oxide/Hydrogel Composites and Their Applications to Adsorptive Removal Congo Red from Aqueous Solution. Journal of Physics: Conference Series; 2019.
27. Radhy ND, Jasim LS. A novel economical friendly treatment approach: Composite hydrogels. Caspian Journal of Environmental Sciences. 2021;19(5):841-52.
28. Abdulsahib WK, Sahib HH, Mahdi MA, Jasim LS. Adsorption Study of Cephalexin Monohydrate Drug in Solution on Poly (vinyl pyrrolidone-acryl amide) Hydrogel Surface. International Journal of Drug Delivery Technology. 2021;11(4):1169-72.
29. Karim AN, Jasim LS. Synthesis and characterization of poly (CH/AA-co-AM) composite: Adsorption and thermodynamic studies of benzocaine on from aqueous solutions. International Journal of Drug Delivery Technology. 2019;9(4):558-62.
30. Mahdi MA, Oroumi G, Samimi F, Dawi EA, Abed MJ, Alzaidy AH, et al. Tailoring the innovative Lu2CrMnO6 double perovskite nanostructure as an efficient electrode materials for electrochemical hydrogen storage application. Journal of Energy Storage. 2024;88.

31. Kianipour S, Razavi FS, Hajizadeh-Oghaz M, Abdulsahib WK, Mahdi MA, Jasim LS, et al. The synthesis of the P/N-type NdCoO3/g-C3N4 nano-heterojunction as a high-performance photocatalyst for the enhanced photocatalytic degradation of pollutants under visible-light irradiation. Arabian Journal of Chemistry. 2022;15(6).
32. Batool M, Haider MN, Javed T. Applications of spectroscopic techniques for characterization of polymer nanocomposite: A review. Journal of Inorganic and Organometallic Polymers and Materials. 2022;32(12):4478-503.
33. Majeed HJ, Idrees TJ, Mahdi MA, Abed MJ, Batool M, Yousefi SR, et al. Synthesis and application of novel sodium carboxy methyl cellulose-g-poly acrylic acid carbon dots hydrogel nanocomposite (NaCMC-g-PAAc/CDs) for adsorptive removal of malachite green dye. Desalination and Water Treatment. 2024:100822.
34. Mojar Alshamusi QK, Hameed KAA, Taher AM, Batool M, Jasim LS. Efficiency of Chitosan-Grafted Poly (Carboxymethyl Cellulose-Co-Acrylamide) Nano Hydrogel for Cadmium (II) Removal: Batch Adsorption Study. Journal of Nanostructures. 2024;14(4):1122-33.
35. Shah A, Arjunan A, Manning G, Batool M, Zakharova J, Hawkins AJ, et al. Sequential novel use of Moringa oleifera Lam., biochar, and sand to remove turbidity, E. coli, and heavy metals from drinking water. Cleaner Water. 2024:100050.